

Formation of recollimation shocks in jets of high-mass X-ray binaries

DooSoo Yoon,^{1,2} Andrzej A. Zdziarski³ and Sebastian Heinz¹

¹*Department of Astronomy, University of Wisconsin-Madison, Madison, WI, USA*

²*Shanghai Astronomical Observatory, Chinese Academy of Sciences, 80 Nandan Road, Shanghai 200030, China*

³*Centrum Astronomiczne im. M. Kopernika, Bartycka 18, PL-00-716 Warszawa, Poland*

Accepted 2015 December 16. Received 2015 November 26; in original form 2015 August 19

ABSTRACT

We study conditions for formation of recollimation shocks in jets interacting with stellar winds in high-mass X-ray binaries. We show the existence of a critical jet power, dependent on the wind rate and velocity and the jet velocity, above which a recollimation shock is not formed. For jet powers below critical, we derive the location of the shock. We show that surface shocks may still exist above the critical power, but only occupy a small volume of the jet and do not significantly alter the jet opening angle. We test these prediction by 3-D numerical simulations, which confirm the existence and the value of the critical power. We apply our results to Cyg X-1 and Cyg X-3.

Key words: acceleration of particles–ISM: jets and outflows–stars: individual: (Cyg X-1, Cyg X-3) – X-rays: binaries.

1 INTRODUCTION

Interaction of an extragalactic jet with a stellar wind of a massive star passing through the jet was considered by Bednarek & Protheroe (1997). As the shock-formation condition, they used the balance of the ram pressures of the forward motion of the jet matter and that of a radial stellar wind. This appears to be the proper approximate condition if the velocity of the star within the jet is much less than the wind velocity. See also Komissarov (1994) for the case of jet interaction with winds of low-mass stars.

The same condition was then used by Dubus, Cerutti & Henri (2010) for formation of a recollimation/reconfinement shock in a jet originating from a compact object and interacting with the stellar wind of a massive donor in a binary system. The condition formulated by Dubus et al. (2010) was then applied to Cyg X-3 by Zdziarski et al. (2012b), who concluded from it that a recollimation shock can be formed only if the initial jet half-opening angle, α_0 , is rather large, $\gtrsim 30^\circ$.

However, the wind-jet collision in a binary system is clearly not head-on. Close to the binary plane, the wind velocity is parallel to the plane, and the jet is launched away from it. In the case of a jet perpendicular to the binary plane, see Fig. 1, the jet and wind velocities are close to perpendicular along the binary plane, and only a velocity component related to the jet opening angle is collinear with the wind.

This effect was taken into account in analytical estimates of Yoon & Heinz (2015), hereafter YH15 (see Perucho & Bosch-Ramon 2008 and Perucho, Bosch-Ramon & Khangulyan 2010 for previous studies of formation of shocks in X-ray binary jets). As the condition of

the ram pressure of the jet being in equilibrium with the wind ram pressure, YH15 took only the jet velocity component collinear with the wind direction in the vicinity of the binary plane, i.e., $v_j \sin \alpha_0$, where v_j is the jet velocity and α_0 is the initial opening angle of the jet. This is applicable only if the recollimation shock takes place at a distance from the jet origin of $z \ll a$, where a is the separation between the binary components. They derived a formula for the location of the recollimation shock in this approximation. YH15 also performed numerical simulations of the jet-wind interaction and found their formula agrees relatively well with the simulation results in the case of a moderate jet power, 10^{37} erg s^{-1} , interacting with a strong wind with a high mass loss rate of $\dot{M}_w = 10^{-5} M_\odot \text{ yr}^{-1}$ and a high wind velocity of $v_w = 2.5 \times 10^8$ cm s^{-1} . However, the assumption that the shock takes place at $z \ll a$ is not applicable for a sufficiently strong jet.

Here, we generalize the calculation of YH15 to the case of an arbitrary jet power. We concentrate on the case of systems in which the jet and orbital axes are aligned; see, e.g., Steiner & McClintock (2012) for a discussion of conditions for the spin-orbit alignment. We test the calculations by means of numerical simulations. We apply our results to jets of the high-mass X-ray binaries Cyg X-1 and Cyg X-3.

2 FORMATION OF RECOLLIMATION SHOCKS

2.1 The setup of the problem

Suppose the jet is expanding with an initial opening angle α_0 . The internal pressure, $p_{j,i} \propto z^{-2\gamma}$ (where γ is the jet's adiabatic index), of the jet drops more rapidly than the jet's lateral ram pressure,

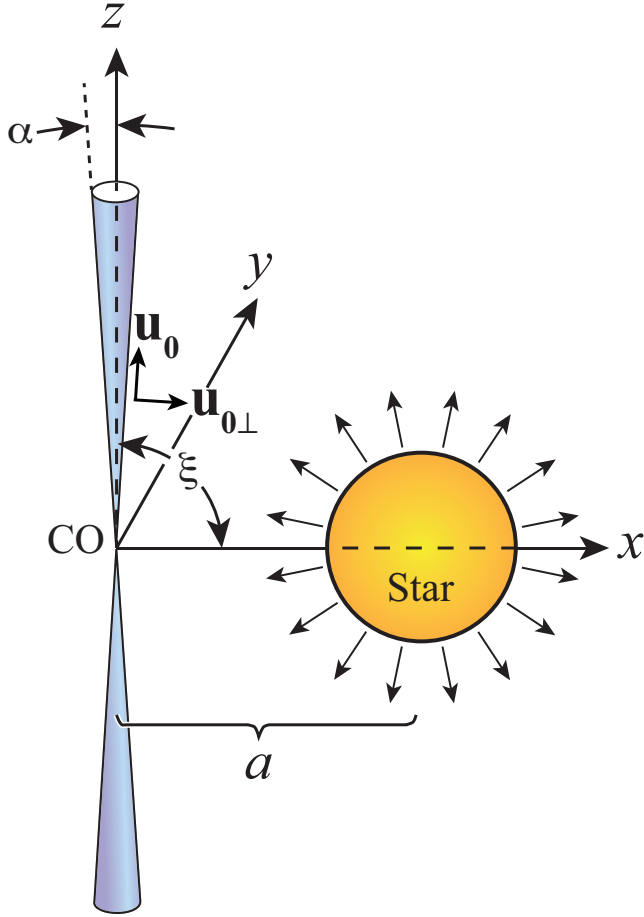


Figure 1. A sketch of a jet originating from a compact object (CO), such as a neutron star or a black hole, and a stellar wind. The jet direction is at an angle, ξ , with respect to the direction from the CO to the star. In the case considered here, the jet is along the z -direction, and thus $\xi = 90^\circ$. The jet’s half-opening angle is α and the separation is a . The star, located at $x_* = a$, emits an isotropic and uniform stellar wind. We also show a unit vector along the contact discontinuity, \mathbf{u}_0 , and one perpendicular to it, $\mathbf{u}_{0\perp}$.

$p_{j,x} \propto z^{-2}$, and the lateral expansion of the jet will become supersonic. Whenever the internal pressure of the jet drops below the total ambient pressure, a shock will be driven laterally into the jet in order to bring the internal pressure into equilibrium with the bow shock.

Such a shock will necessarily reduce the lateral expansion velocity of the jet (using the free energy in the jet’s expansion to increase the internal energy of the jet fluid), and may thus be called a “recollimation” shock. Below, we will distinguish “strong recollimation shocks” from “weak” or “surface shocks”. A strong recollimation shock will convert *most or all* of the lateral expansion energy (a fraction $\sim \sin^2 \alpha_0$ of the total kinetic energy of the jet) into particle heating and/or acceleration, with important observational consequences for, e.g., the high-energy emission from particles accelerated in this shock. A surface shock will reduce the opening angle by a small amount, $\Delta\alpha \ll \alpha$, sufficient to raise the pressure to the ambient value, but dissipating only a small fraction of the jet’s lateral kinetic energy.

To estimate the change in opening angle of the jet, we consider ram pressure balance of a supersonic spherical wind colliding with a supersonic conical jet. The collision will take place on the side

of the jet exposed to the wind. At a given point along the jet, this can be approximated as two streams colliding at some angle. This collision will lead to formation of two shocks – one into the wind (which we will refer to as the bow shock) and one into the jet (the recollimation shock).

We define the coordinate system with the x - y plane coinciding with the binary plane, and the z axis perpendicular to it, see Fig. 1 and, for the sake of simplicity, analyse the shock properties in the x - z plane (where the bow shock and thus the recollimation shock will be strongest). We place the star centre at $x_* = +a$ and the jet origin at $x = 0$. Following YH15, we perform all calculations in the non-relativistic approximation.

The contact discontinuity will be parallel to the post-shock velocities of the jet and the wind. In the frame of the contact discontinuity, ram pressure balance takes the form of, e.g., eq. (11) of Nalewajko & Sikora (2009),

$$\rho_w v_{w\perp}^2 = \rho_j v_{j\perp}^2, \quad (1)$$

where ρ_w, ρ_j are the densities of the wind and the jet, respectively, and $v_{w\perp}$ and $v_{j\perp}$ are the wind and jet velocity components perpendicular to the contact discontinuity, respectively. We can define a unit vector along the contact discontinuity and a vector perpendicular to it as

$$\begin{aligned} \mathbf{u}_0 &= (\sin \alpha', 0, \cos \alpha') = (x_0, 0, \sqrt{1 - x_0^2}), \\ \mathbf{u}_{0\perp} &= (-\cos \alpha', 0, \sin \alpha') = (-\sqrt{1 - x_0^2}, 0, x_0), \end{aligned} \quad (2)$$

which defines x_0 and the inclination angle α' of the contact discontinuity relative to the initial jet axis. Then $v_{w\perp} = \mathbf{v}_w \cdot \mathbf{u}_{0\perp}$ and $v_{j\perp} = \mathbf{v}_j \cdot \mathbf{u}_{0\perp}$. We can then solve equation (1) for $x_0(z)$. The trajectory assuming the post-shock jet fluid follows the contact discontinuity is then given by the solution of $dx/dz = \tan \alpha' = x_0 / \sqrt{1 - x_0^2}$. We note that we do not impose conservation of energy and momentum, assuming that energy can be dissipated and radiated and the wind flow can continue around the jet. Also, the above condition is not satisfied close to the jet origin because the perpendicular velocity components are not supersonic. We neglect this effect since we are concerned with regions where the velocity components are supersonic.

The jet is initially freely expanding and conical with the initial semi-opening angle, α_0 , related to its initial Mach number, \mathcal{M}_j (YH15). The lateral ram pressure of the jet, i.e., along the x direction, is

$$p_{j,x} = \rho_j \tan^2 \alpha_0 v_j^2 = \frac{P_j}{\pi z^2 v_j}, \quad (3)$$

where we assumed v_j to be constant. In the second equality, we have expressed the pressure in terms of the kinetic power of the jet+counterjet in the rest mass motion, $P_j = \pi \rho_j v_j^3 z^2 \tan^2 \alpha_0$. Then, $p_{j,x}$ is independent of the jet opening angle. Note that we use the power of both jets here, which is of interest when considering the energy budget of the system, in particular comparing the jet and accretion powers. The same convention was used by YH15.

On the other hand, the ram pressure of the wind in its motion component along the binary plane is

$$p_{w,x} = \rho_w v_{w,x}^2 = \frac{\dot{M}_w v_w}{4\pi a^2} \left(\frac{a^2}{a^2 + z^2} \right)^2, \quad (4)$$

where \dot{M}_w is the mass-loss rate in the wind and v_w is its velocity, assumed constant along the jet. The second factor on the right-hand side appears due to both the wind density and $v_{w,x}^2/v_w^2$ decreasing as

$a^2/(a^2 + z^2)$. This factor is not present in eq. (8) of YH15 because they consider only shock formation close to the binary plane. However, as we show below, recollimation shocks in jets of HMXBs can take place at distances comparable to the binary separation, or not happen at all, in which cases that term is important.

We solve for the inclination angle of the contact discontinuity:

$$\tan \alpha' = \tan \alpha_0 \frac{\sqrt{4P_j / (\dot{M}_w v_w v_j)} (a^2 + z^2) - az}{\sqrt{4P_j / (\dot{M}_w v_w v_j)} (a^2 + z^2) + z^2 \tan \alpha_0}, \quad (5)$$

with a deflection angle at the leading edge of the jet of $\Delta\alpha = \alpha_0 - \alpha'$.

2.2 Strong recollimation shocks

The formation of a strong recollimation shock corresponds to the direction defined by equation (1) being substantially different from the direction of the jet boundary facing the star, i.e., $\Delta\alpha \geq \alpha$. The limiting case for the formation of a strong shock is thus $\alpha' = x_0(z) = 0$, which corresponds to the treatment given in section 3.2 of YH15.

Equating the pressures leads to a quadratic equation in $(z/a)^2$. The equation has real positive solutions for the jet kinetic power satisfying

$$P_j \leq P_{\text{cr}} \equiv \frac{1}{16} \dot{M}_w v_w v_j. \quad (6)$$

Note that P_{cr} is independent of the jet opening angle.

More generally, in the case of jets inclined with respect to the orbit, it is straightforward to show that the shock formation criterion is

$$P_j \leq P_{\text{cr}} \left(\frac{1 + \cos \xi}{\sin \xi} \right)^2, \quad (7)$$

where ξ is the inclination angle between the jet and the orbital separation vector, \mathbf{a} . Note that the critical power is different for approaching and receding half of an inclined jet, as the sign of $\cos \xi$ changes from positive to negative as a jet tilts further than 90° away from the companion, because the wind ram pressure decreases and lower powers are sufficient to suppress the formation of a recollimation shock.

If the condition in equation (6) is satisfied, the jet lateral ram pressure, decreasing as z^{-2} , becomes equal to the corresponding wind ram pressure at some point z_1 along the jet, and a strong recollimation shock forms. Thus, the lower solution corresponds to the condition of shock formation. The shock location is then given by

$$\left(\frac{z_1}{a} \right)^2 = \delta - 1 - \sqrt{\delta^2 - 2\delta}, \quad \delta \equiv \frac{\dot{M}_w v_w v_j}{8P_j} \geq 2, \quad (8)$$

$$\simeq 1/(2\delta), \quad \delta \gg 1, \quad (9)$$

where the approximate equation (9) corresponds to the solution given by YH15 in their eq. (9). At the critical point of $P_j = P_{\text{cr}}$, there is one solution at $z_1 = a$. Thus, under the adopted approximations, a strong recollimation shock never forms at $z > a$. If $P_j > P_{\text{cr}}$, the jet lateral ram pressure will be always greater than that of the wind.

Once the shock takes place, the jet is no longer conical and freely expanding [such that equation (5) no longer applies], but instead its thickness follows from pressure equilibrium between the jet and the wind bow shock, see section 4.1 of YH15. However, equations (3–4) still remain valid. Thus, the jet becomes again freely expanding above z_2 given by the upper solution of the quadratic equation obtained by equating these two equations,

$$\left(\frac{z_2}{a} \right)^2 = \delta - 1 + \sqrt{\delta^2 - 2\delta}, \quad \delta \geq 2. \quad (10)$$

2.3 Surface shocks

Even if the strong shock criterion is not satisfied, a shock may still form if the internal pressure of the jet drops below the bow shock pressure. In that case, the maximum deflection angle, $\Delta\alpha$, from equation (5) is small compared to α . While such a surface shock will necessarily be highly oblique and weak compared to a recollimation shock, it is important to note that it may still be a strong shock in the sense of having a large Mach number and changing the entropy of the gas.

In the limit of $\Delta\alpha \ll \alpha_0$, the location of the maximum relative dynamic pressure, where $\Delta\alpha$ is maximized, is

$$z_{\text{maz}} \approx \frac{a}{\cos \alpha_0} (1 + \sin \alpha_0) \simeq a, \quad (11)$$

and, to the lowest order, the maximum deflection angle becomes

$$\Delta\alpha \approx -\alpha_0 \sqrt{\frac{P_{\text{cr}}}{P_j}}, \quad (12)$$

valid in the regime $P_j \gg \dot{M}_w v_w v_j$ (and assuming the small angle approximation for α_0).

The pressure behind such a surface shock is still given by the bow shock pressure, $p_{\text{shock}} \sim M_w^2 v_w^2 / (16\pi a^2)$ (the same as in the case of a strong recollimation shock). The volume occupied by the shock is roughly

$$V_{\text{shock}} \sim \frac{2\pi a^3}{3} \alpha_0 \Delta\alpha \simeq \frac{2\pi}{3} \alpha_0^2 a^3 \sqrt{\frac{P_{\text{cr}}}{P_j}}. \quad (13)$$

This situation is illustrated in Fig. 2, which shows the structure of the bow shock and the moderate oblique shock driven into the jet.

Since we would expect the non-thermal emission from such a shock to be proportional to the volume of the shock and some function of the pressure, the total non-thermal emission from the shock should be proportional to $\sqrt{\dot{M}_w v_w v_j / P_j}$, i.e., it decreases with the square root of the jet power for super-critical jets that do not form strong recollimation shocks and for otherwise identical jet and wind parameters.

3 COMPARISON WITH SIMULATIONS

3.1 Methods

In order to test the predictions for the formation of recollimation shocks, we carried out 3-D hydrodynamic simulations using FLASH 3.3 grid-based adaptive-mesh hydrodynamics code (Fryxell et al. 2000) for testing the conditions in which a recollimation shock forms, using the same method as that of YH15. In YH15, the jet was modelled by a cylindrical nozzle with inflow-boundary conditions at the surface, injecting a bipolar outflow with a prescribed energy, mass, and momentum flux. This cylindrical nozzle was required to set a slow lateral outflow from the side walls of the cylinder due to the numerical stability. The injected materials from the lateral outflow interact with the stellar wind, losing the momentum and falling back to the jet, which yields artificial mass-loading on the jet. In the jet model with $P_j \leq 10^{37}$ erg s $^{-1}$, the amount of the mass-loading and its effect on the jet bending are negligible. However, as the jet kinetic power increases, the mass-loading becomes noticeable and this effect should be taken into consideration.

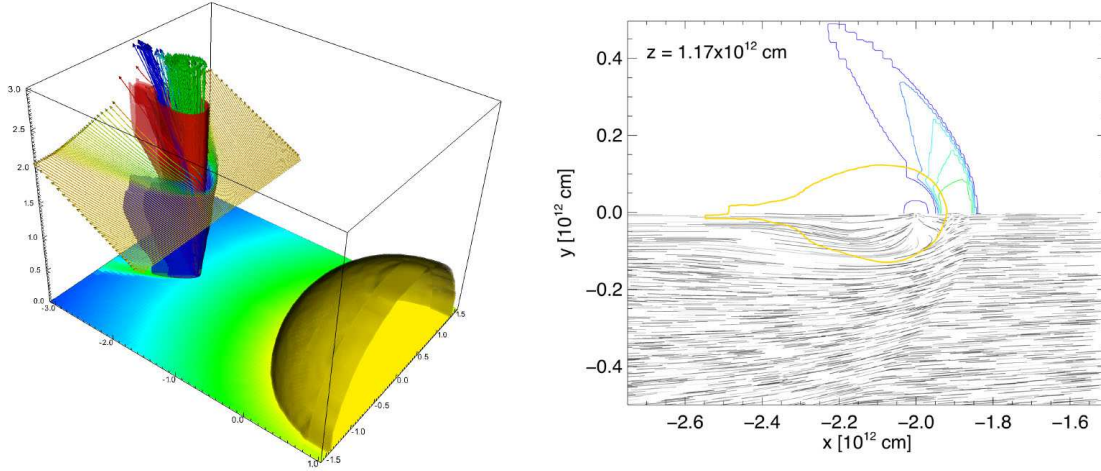


Figure 2. Left panel: Visualization of the P3e37 simulation. *Red contour surface*: section of the jet boundary; *blue contour surface*: section of the bow shock; *yellow contour surface*: surface of the star; *bottom surface*: slice through the temperature of the stellar wind and bow shock; *vectors*: stream lines sampling the jet and the stellar wind/bow shock. The axes are in units of 10^{12} cm. Right panel: slice through P3e37 simulation at $z = 1.17 \times 10^{12}$ cm showing the structure of the bow shock and the formation of a surface shock on the leading edge of the jet; *top part*: five pressure contours linearly spaced between 13 and 80 per cent of the theoretical stagnation point pressure of the bow shock; overlaid in yellow is the approximate location of the contact discontinuity; *bottom part*: 2-D velocity streamlines in the x - y plane showing the deflection of the wind in the bow shock and the acceleration of jet material away from the stagnation point behind the surface shock and in the expansion wave in the down-wind region of the jet.

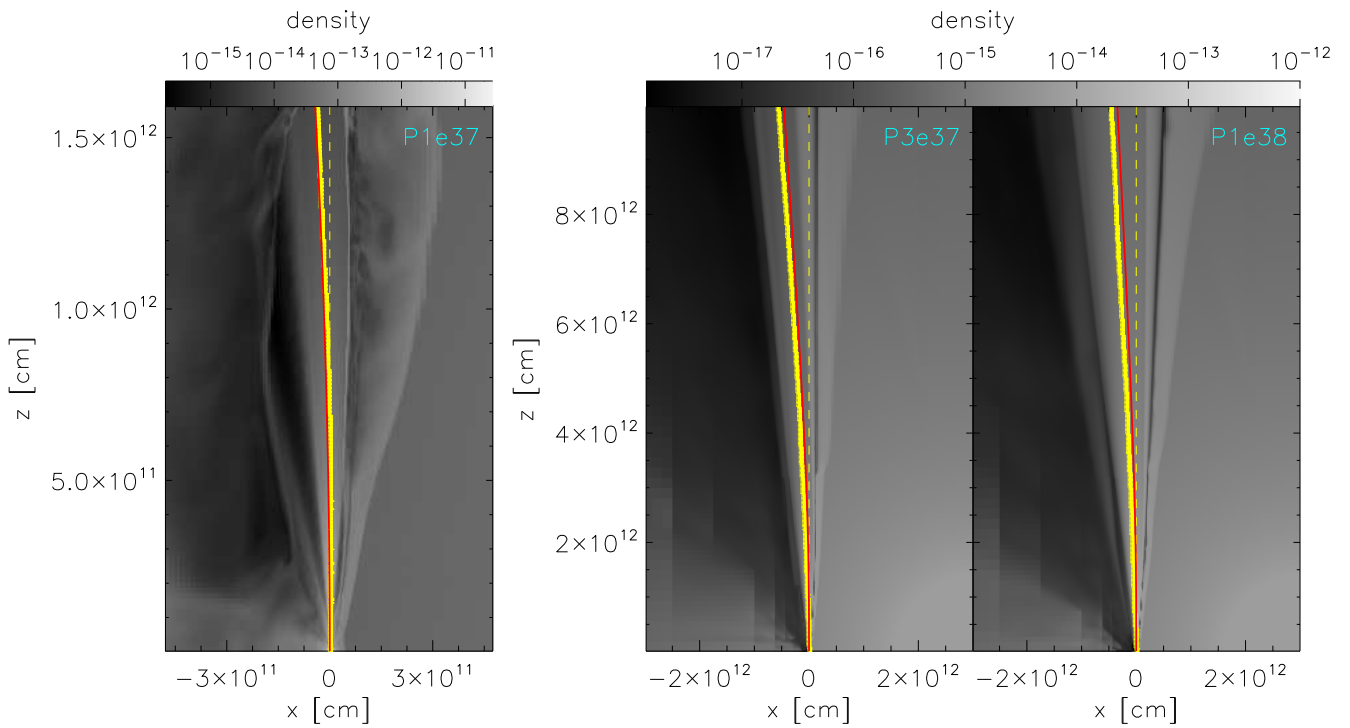


Figure 3. The density contour maps in x - z plane for the P1e37 (left), P3e37 (middle) and P1e38 (right) models. The P1e37 model is from YH15, in which the considered length along the jet is an order of magnitude smaller than that of the P3e37 and P1e38 models. The vertical line up from the black hole position is shown by yellow dashes. The thick yellow line represents the identified jet centre from simulations and the thick red line represents the analytic approximation to the jet trajectory.

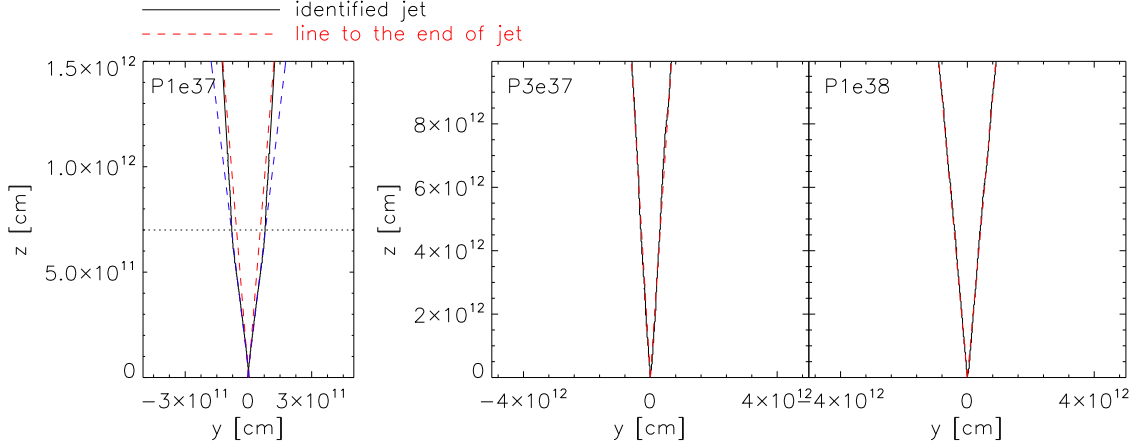


Figure 4. The jet in the y -direction as a function of z . The black solid line represents the jet identified from the simulations. The straight line between the black hole and the end of the jet is shown by the red dashes. In the P1e37 model, the blue dashes are straight lines that follow the initial opening angle, $\alpha_0 \simeq 6.5^\circ$, and the horizontal dotted line represents the location of the recollimation shock.

To eliminate the side effects of the artificial outflow, we implement the jet nozzle within the lower boundary instead of an interior grid.

Our numerical configuration is similar to that in Perucho & Bosch-Ramon (2008) and Perucho et al. (2010), which showed jet-wind interaction in massive X-ray binaries by using 2-D and 3-D simulations, respectively. They concluded that jet is likely bent and disrupted for jet kinetic power $\lesssim 10^{36}$ erg s^{-1} by the ram pressure of stellar wind from nearby O-type star, which is also consistent with YH15.

The parameters of the jet and stellar wind are the same as in YH15, except for the jet kinetic power. Namely, we use $v_j = 3 \times 10^9$ cm s^{-1} , $v_w = 2.5 \times 10^8$ cm s^{-1} , $\dot{M}_w = 10^{-5} M_\odot$ yr $^{-1}$, $a = 3 \times 10^{12}$ cm, and the Mach number of $\mathcal{M}_j = 30$, which corresponds to one of the two recollimation-shock cases studied by YH15. For the assumed v_j , v_w , and \dot{M}_w , the critical jet power, equation (6), is $P_{cr} \simeq 3.0 \times 10^{37}$ erg s^{-1} .

In addition to the recollimation case considered by YH15, with a kinetic power of $P_j = 10^{37}$ erg s^{-1} (P1e37), we have carried out two sets of runs with $P_j = 3 \times 10^{37}$ and 10^{38} erg s^{-1} , which we denote as P3e37 and P1e38, respectively. In our coordinate system, the jet origin and the star are located at $x_{CO} = 0$ and $x_* = a$, respectively. A volume rendering and contour plot of the P3e37 simulations is shown in Fig. 2 for illustration.

3.2 Jet bending

In the presence of a stellar wind, the jet is bent by a transverse pressure gradient that the wind drives around the jet (see Fig. 2). The bending has to be taken into account for identification of a recollimation shock. Therefore, we identify the jet centre in order to be able to estimate the jet thickness in the y -direction, see YH15. Fig. 3 shows how the jet is deviating from its initial direction along the z axis. The yellow thick lines show the jet centre identified in the simulation data. We ensure that the simulations have evolved for a sufficiently long time for the initial bow shock of the jet to propagate well beyond the region of interest, allowing for interaction directly with the stellar wind.

For the analysis of jet-bending, we assume the jet remains conical with a fixed jet opening angle, α_0 . This is in contrast to the analytic jet model in YH15, in which the jet is confined by pres-

sure equilibrium between the jet and the wind (red solid line of the P1e37 model in Fig. 3), and thus the jet is not conical. The former is appropriate for powerful jets and prior to the formation of a strong recollimation shock, the latter is appropriate for weaker and strongly bent jets beyond the location of the recollimation shock. As we will show in Section 3.3 below, the more powerful jets in our case study (the P3e37 and P1e38 models) are not substantially recollimated, and have approximately constant opening angle, α_0 , so we adopt a conical shape for the analytic jet model.

The derivation is similar to that of YH15. Assuming that the longitudinal jet velocity is constant and $\mathcal{M}_j \gg 1$, the longitudinal jet momentum per unit jet length can be calculated by

$$\Phi_j = \int dA_\perp \rho_j v_j = \frac{P_j}{v_j^2}, \quad (14)$$

where dA_\perp is the area perpendicular to the initial jet direction. The transverse wind momentum per unit jet length accumulated by the jet as a function of z is

$$\Delta\Phi_w = \frac{1}{v_j} \int_0^\infty dz' v_{w,x}^2(z') \rho_w(z') h(z'), \quad (15)$$

where $h(z) = 2z \tan \alpha_0$ is the jet width. Equation (15) can be readily integrated to

$$\Delta\Phi_w = \frac{v_{w,0} \dot{M}_w \tan \alpha_0}{4\pi v_j} \frac{z^2}{a^2 + z^2}. \quad (16)$$

In the first-order approximation, the jet bending angle, ψ , can be derived by the ratio between the accumulated transverse momentum and the longitudinal momentum as a function of z ,

$$\psi(z) \simeq \frac{\Delta\Phi_w}{\Phi_{m,j}} = \frac{v_{w,0} v_j \dot{M}_w \tan \alpha}{4\pi P_j} \frac{z^2}{a^2 + z^2}. \quad (17)$$

At $z^2 \gg a^2$, the bending angle reaches its asymptotic value. In the small-angle approximation, we can derive the analytic jet trajectory through $d(x - x_{CO})/dz = \tan \psi$. Analytic trajectories derived for the simulations are shown by the thick red lines in Fig. 3. They show good agreement with the simulation results (thick yellow lines), indicating that our simple analytic model can describe the bending jet. The bending angle is similar between the P3e37 and P1e38 models, because although the P1e38 model has a jet kinetic power

about 3.3 times larger than that of the P3e37 one, the opening angle in P1e38 is also 2.4 times larger than that of P3e37 (see Section 3.3).

3.3 Recollimation

YH15 studied the appearance of a recollimation shock at $P_j = 10^{37}$ erg s $^{-1}$, in which case the shock takes place at $z \approx 7 \times 10^{11}$ cm $\ll a$ (horizontal dotted line in the left panel of Fig. 4).

In YH15, the jet was found to initially expand freely, its lateral expansion proceeding until the lateral ram pressure of the jet dropped below the wind ram pressure, where a recollimation shock occurred (independent of the initial jet opening angle and the jet Mach number). Beyond the shock, the jet evolved adiabatically in pressure equilibrium between the jet and the wind bow shock.

However, with increasing jet power, the shock takes place at increasingly larger z or does not occur at all, as found analytically in Section 2. To check for the presence of a recollimation shock, we measured the jet width facing the star, i.e., along the y -direction. We measured the width along the identified jet centre (yellow thick line in Fig. 3). The black solid lines in Fig. 4 show that the measured jet width increases almost linearly, and no recollimation shock is apparent. The opening angles are $\alpha(\text{P3e37}) \approx 3.4^\circ$ and $\alpha(\text{P1e38}) \approx 8^\circ$.

In order to determine whether the contact discontinuity is measurably misaligned with the initial jet opening angle, we compare the jet trajectories with straight lines connecting the black hole with the edge of the jet at the upper limit of the analysis box (red dashes in Fig. 4). Then we calculate the (squared) fractional deviation as a function of z ,

$$\sigma^2(z) \equiv [y_j^2(z) - y_j^2(z)]/y_{j0}^2(z), \quad (18)$$

where y_j and y_{j0} are the positions of jet edge for the simulations and the straight line, respectively. Fig. 5 shows that for P1e38, the identified jet boundary is in good agreement with the straight line, indicating a conical shape of jet and the absence of a recollimation shock.

The jet in P3e37 also has an overall almost conical shape, but there is substantial negative deviation from this shape at $z \lesssim 3 \times 10^{12}$ cm. This shows that a surface shock does take place around $z \sim a$, confirming the analytic prediction of Section 2 for the shock location around the separation at $P_j \gtrsim P_{\text{cr}}$. The jet at $z \lesssim a$ has then an opening angle $\alpha > 3.4^\circ$.

These results are in a good agreement with the predictions of equation (6) for the wind properties that we have used in this work. According to equation (6), the critical jet power, above which there should be no strong recollimation shocks, equals $P_j \approx 3.0 \times 10^{37}$ erg s $^{-1}$. From our simulations, there is a strong shock at $P_j = 10^{37}$ erg s $^{-1}$, a mild shock at $P_j = 3 \times 10^{37}$ erg s $^{-1}$, and an no measurable change in opening angle for $P_j = 10^{38}$ erg s $^{-1}$.

While the analysis presented in this paper focuses on the shock formed by the interaction of the leading edge of the jet with the stellar wind bow shock, the simulations allow a description of the down-wind half of the jet dynamics as well. As can be seen in Fig. 2, the thermal pressure of the bow shock drops to low values in the shadow of the jet, leading to the formation of an expansion fan that accelerates the jet and wind fluid into the evacuated region behind the jet. In some instances, this very low-density material may form a shock upon convergence on the x - z plane behind the jet, which is the reason for the appearance of denser gas in the wake of the jet in Fig. 3.

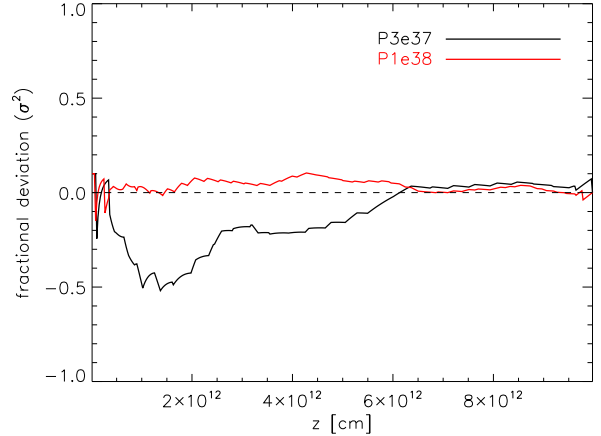


Figure 5. The squared fractional deviation between the jet edge measured in simulations in the y -direction and the straight line connecting the black hole and the jet end, given by σ^2 defined by equation (18). The black and red colours correspond to the P3e37 and P1e38 models, respectively. The horizontal dashed line indicates no deviation.

4 JETS IN CYG X-1 AND CYG X-3

We can check the implications of the above results for two high-mass X-ray binaries with jets. Cyg X-1 contains a black hole with the mass of $\approx 16M_\odot$ (Orosz et al. 2011; Ziółkowski 2014). The mass of the donor is disputed, Ziółkowski (2014) estimates it as $\approx 27M_\odot$. Then, the separation equals 3.2×10^{12} cm. Cyg X-1 has a steady compact jet in the hard state (Stirling et al. 2001).

The current best estimates of the relevant parameters of Cyg X-1 are the mass-loss rate in the hard state of $\dot{M}_w \approx 2.6 \times 10^{-6}M_\odot$ yr $^{-1}$ (Gies et al. 2003), its asymptotic velocity of $v_w \approx 1.6 \times 10^8$ cm s $^{-1}$ (Gies & Bolton 1986) and the relatively uncertain jet velocity of $v_j \approx 0.6c$ (Stirling et al. 2001; Gleissner et al. 2004; Malzac, Belmont & Fabian 2009). These parameters correspond to the critical power of $P_{\text{cr}} \approx 3 \times 10^{37}$ erg s $^{-1}$. This is within the estimated $P_j \approx (1-7) \times 10^{37}$ erg s $^{-1}$ (for the jet+counterjet) from the optical nebula presumably powered by the jet (Sell et al. 2015; see also Gallo et al. 2005; Russell et al. 2007). Thus, a recollimation shock can occur in the hard-state jet of Cyg X-1. The location of the shock is given by equation (8). At $P_j = 10^{37}$ erg s $^{-1}$, the shock takes place at $z = 0.32a$. The jet power of Cyg X-1 has also been estimated in several theoretical models of Zdziarski, Lubiński & Sikora (2012a), Malyshev, Zdziarski & Chernyakova (2013), Zdziarski et al. (2014) and YH15. For almost all of the model power was $\ll P_{\text{cr}}$ (the only exception was one model in Malyshev et al. 2013, which those authors themselves considered unlikely).

Although it is likely that Cyg X-3 also contains a black hole, the current solution for its mass also allows the presence of a neutron star (Zdziarski, Mikołajewska & Belczyński 2013). We adopt $\dot{M}_w \approx 7 \times 10^{-6}M_\odot$ yr $^{-1}$ (see Zdziarski et al. 2013 and references therein), $v_w \approx 1.6 \times 10^8$ cm s $^{-1}$ (van Kerkwijk et al. 1996), $v_j \approx 0.5c$ (Zdziarski et al. 2012b; Dubus et al. 2010) and $a = 2.4 \times 10^{11}$ cm (assuming the total mass of $13M_\odot$, Zdziarski et al. 2013). We then obtain $P_{\text{cr}} \approx 6.6 \times 10^{37}$ erg s $^{-1}$. This is similar to, or somewhat below, the power estimate of Zdziarski et al. (2012b) during periods of strong γ -ray emission in the soft state (Fermi LAT Collaboration 2009; Tavani et al. 2009), based on the γ -ray luminosity.

Thus, a strong recollimation shock may occur in the hard-state

jet of Cyg X-1 and the soft state of Cyg X-3 during periods of strong γ -ray emission. Since $P_j \sim P_{cr}$ in both cases, the shock location is close to the maximum possible position of $z \sim a$. This, in fact, agrees with the analyses of Dubus et al. (2010) and Zdziarski et al. (2012b) for Cyg X-3, based on modelling of the γ -ray emission.

In Cyg X-1, the formation of a recollimation shock at $z \lesssim a$ may thus explain an apparent departure of the structure of the jet from the standard model of Blandford & Königl (1979), see Heinz (2006), Zdziarski (2012) and Zdziarski et al. (2012a). Namely, the observed resolved fraction of the 8.4-GHz jet emission (Stirling et al. 2001) implies the location of the onset of the optically-thin synchrotron radio emission at $z \sim 10^{14}$ cm (Heinz 2006), which appears not compatible with the observed orbital modulation of the 15-GHz emission having a depth of ≈ 30 per cent (Zdziarski 2012). This modulation results from free-free absorption in the wind, and its large depth requires a substantial difference between the paths through the wind between the superior and inferior conjunctions, which, in turn, implies that a large part of the radio emission originates from $z \lesssim a$ (Zdziarski 2012). A recollimation shock at $z \lesssim a$ can lead to strong dissipation and radio emission (spatially unresolved) on top of the remainder of the jet emission, explaining the above discrepancy.

On the other hand, we note that Cyg X-1 in its hard state is much less radio loud than Cyg X-3 in its hard state. For the radio loudness defined as the ratio of νL_ν at 15 GHz to the bolometric luminosity (dominated by X-rays), both in units of the Eddington luminosity, this striking difference is illustrated in fig. 7 of Zdziarski, Segreto & Pooley (2016). This ratio is $\sim 3 \times 10^{-8}$ and $\sim 10^{-6}$ in Cyg X-1 and Cyg X-3, respectively. This difference by a factor of ~ 30 could be explained by the shock in the former and the latter being weak and strong, respectively.

Finally, we stress that bright radio jets are common also in low-mass X-ray binaries, e.g., Fender (2006), where no stellar wind-jet interaction occurs. Thus, the formation of a recollimation shock, either strong or weak, is clearly not a condition for a jet radio emission; however, it is likely to modify the radio emissivity profile with respect to that corresponding to the absence of such a shock.

5 CONCLUSIONS

We have derived an analytical criterion for the existence of recollimation shocks in jets in high-mass X-ray binaries. We have tested it with 3-D numerical simulations and have found a good agreement with the analytic predictions. According to this criterion, a recollimation shock in jets of high-mass X-ray binaries can exist only below the critical jet power proportional to the mass-loss rate, given by equation (6). Below that critical jet power, the position of the shock is given by equation (8). Both the condition for shock formation and the shock location are independent of the initial jet opening angle. Above the critical power, a highly oblique surface shock may still form to raise the jet's internal pressure to the bow shock pressure, but such a shock will only change the opening angle by a small amount and will only occupy a small fraction of the jet's volume.

We have applied our results to the high-mass binaries Cyg X-1 and Cyg X-3. The presence of a recollimation shock is likely in both of those objects. In the latter system, we can identify the position of the shock with the region of γ -ray emission. The large difference in the radio loudness between those objects can be ex-

plained by the presence of a weak and strong shock in Cyg X-1 and Cyg X-3, respectively.

ACKNOWLEDGMENTS

We thank Marek Sikora for valuable discussions, and Guillaume Dubus and the referee for valuable comments. AAZ has been supported in part by the Polish NCN grants 2012/04/M/ST9/00780 and 2013/10/M/ST9/00729. DSY and SH acknowledge support from the National Science Foundation through grant AST 0908690. This work used the Extreme Science and Engineering Discovery Environment (XSEDE), which is supported by National Science Foundation grant number ACI-1053575.

REFERENCES

- Bednarek W., Protheroe R. J., 1997, *MNRAS*, 287, L9
 Blandford R. D., Königl A., 1979, *ApJ*, 232, 34
 Dubus G., Cerutti B., Henri G., 2010, *MNRAS*, 404, L55
 Fender R., 2006, in Lewin W. van der Klis M., eds., *Compact stellar X-ray sources*. Cambridge Univ. Press, p. 381
 Fermi LAT Collaboration, 2009, *Science*, 326, 1512
 Fryxell, B., et al., 2000, *ApJS*, 131, 273
 Gallo E., Fender R., Kaiser C., Russell D., Morganti R., Oosterloo T., Heinz S., 2005, *Nature*, 436, 819
 Gies D. R., Bolton C. T., 1986, *ApJ*, 304, 389
 Gies D. R. et al., 2003, *ApJ*, 583, 424
 Gleissner T., et al., 2004, *A&A*, 425, 1061
 Heinz S., 2006, *ApJ*, 636, 316
 Komissarov S. S., 1994, *MNRAS*, 269, 394
 Malyshev D., Zdziarski A. A., Chernyakova M., 2013, *MNRAS*, 434, 2380
 Malzac J., Belmont R., Fabian A. C., 2009, *MNRAS*, 400, 1512
 Nalewajko K., Sikora M., 2009, *MNRAS*, 392, 1205
 Orosz J. A., McClintock J. E., Aufdenberg J. P., Remillard R. A., Reid M. J., Narayan R., Gou L., 2011, *ApJ*, 742, 84
 Perucho M., Bosch-Ramon V., 2008, *A&A*, 482, 917
 Perucho M., Bosch-Ramon V., Khangulyan D., 2010, *A&A*, 512, L4
 Russell D. M., Fender R. P., Gallo E., Kaiser C. R., 2007, *MNRAS*, 376, 1341
 Sell P. H., et al., 2015, *MNRAS*, 446, 3579
 Steiner J. F., McClintock J. E., 2012, *ApJ*, 745, 136
 Stirling A. M., Spencer R. E., de la Force C. J., Garrett M. A., Fender R. P., Ogle R. N., 2001, *MNRAS*, 327, 1273
 Tavani M., et al., 2009, *Nature*, 462, 620
 Towns J., et al., 2014, *Computing in Science & Engineering*, 16, 62
 van Kerkwijk M. H., Geballe T. R., King D. L., van der Klis M., van Paradijs J., 1996, *A&A*, 314, 521
 Yoon D., Heinz S., 2015, *ApJ*, 801, 55 (YH15)
 Zdziarski A. A., 2012, *MNRAS*, 422, 1750
 Zdziarski A. A., Lubiński P., Sikora M., 2012a, *MNRAS*, 423, 663
 Zdziarski A. A., Sikora M., Dubus G., Yuan F., Cerutti B., Ogorzałek A., 2012b, *MNRAS*, 421, 2956
 Zdziarski A. A., Mikołajewska J., Belczyński K., 2013, *MNRAS*, 429, L104
 Zdziarski A. A., Pjanka P., Sikora M., Stawarz Ł., 2014, *MNRAS*, 442, 3243

Zdziarski A. A., Segreto A., Pooley G. G., 2016, MNRAS, in
press, arXiv:1508.02049
Ziółkowski J., 2014, MNRAS, 440, L61